

GCPV: Guided Concept Projection Vectors for the Explainable Inspection of CNN Feature Spaces

Georgii Mikriukov^{1,2}Gesina Schwalbe¹Christian Hellert¹Korinna Bade²¹Continental AG²Hochschule Anhalt¹{firstname.lastname}@continental.com²{firstname.lastname}@hs-anhalt.de

Abstract

For debugging and verification of computer vision convolutional deep neural networks (CNNs) human inspection of the learned latent representations is imperative. Therefore, state-of-the-art eXplainable Artificial Intelligence (XAI) methods globally associate given natural language semantic concepts with representing vectors or regions in the CNN latent space supporting manual inspection. Yet, this approach comes with two major disadvantages: They are locally inaccurate when reconstructing a concept label and discard information about the distribution of concept instance representations. The latter, though, is of particular interest for debugging, like finding and understanding outliers, learned notions of sub-concepts, and concept confusion. Furthermore, current single-layer approaches neglect that information about a concept may be spread over the CNN depth. To overcome these shortcomings, we introduce the local-to-global Guided Concept Projection Vectors (GCPV) approach: It (1) generates local concept vectors that each precisely reconstruct a concept segmentation label, and then (2) generalizes these to global concept and even sub-concept vectors by means of hierarchical clustering. Our experiments on object detectors demonstrate improved performance compared to the state-of-the-art, the benefit of multi-layer concept vectors, and robustness against low-quality concept segmentation labels. Finally, we demonstrate that GCPVs can be applied to find root causes for confusion of concepts like “bus” and “truck”, and reveal interesting concept-level outliers. Thus, GCPVs pose a promising step towards interpretable model debugging and informed data improvement.

1. Introduction

Ensuring and transparently debugging properties like safety and fairness of trained opaque machine learning models like CNNs has become an essential challenge [4, 15, 29, 43], manifested both in legal obligations [12, 23] as well as in-

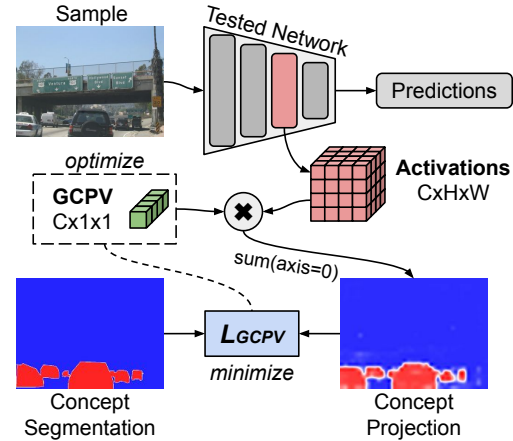


Figure 1. The optimization of a GCPV for a single sample.

dustrial standards [1, 30–32]. While intrinsically interpretable models may be preferable [61], this may not be feasible due to performance trade-offs [52, 80] or incomplete knowledge during design- and train-time [75]. Against this background, it is imperative for quality assurance and debugging [3] to not only understand the black-box behavior of trained CNNs [39, 47, 59], but also the learned knowledge encoded in their feature spaces [29, 63, 64]. To tackle this, state-of-the-art approaches connect vectors or regions in the feature space with semantic concepts, i.e., human-understandable notions from natural language like object classes such as “bus” or “truck” [13, 18, 22, 35, 64]. Amongst these, unsupervised methods for CNN-defined concept discovery like [17, 22, 55, 78] identify the most discernible patterns within the CNN latent spaces. These, however, may not be human-understandable, limiting use in targeted analysis. In contrast, supervised methods like [5, 13, 18, 35] aim to associate a *user-defined* concept, provided via a dataset of inputs with concept segmentation labels, with CNN-learned knowledge. Notable base work is Net2Vec [18] that represents a concept by a vector of weights for CNN filters (the concept vector), interpreted as a direction in latent space; given a concept dataset, these

weights are optimized to reconstruct the concept labels from filter activation maps by linear combination. This can similarly be applied to concept class labels [35]; and be extended to radial kernels instead of point vectors [13].

While these approaches seem to solve feature space debugging, they strictly assume that learned information about a concept can be represented by a *single* point or fixed-shaped radial region in a *single* CNN latent space. This fails to capture complexity of state-of-the-art CNN latent spaces: (1) concepts can span *multiple* regions in feature space, leading to instability of purely global concept vectors [13, 49], while (2) being *distributed* with varying density over the feature space giving rise to outliers; moreover, (3) concept information, e.g., abstraction levels like texture and shape, may be spread across several layers [18, 19, 50, 63]. Capturing such nuances of CNN knowledge is needed to understand, e.g., what concept samples are *outliers* (i.e., hard cases or mismatches between human and machine concept understanding), where concepts overlap potentially leading to *concept confusion*, and whether a concept gives rise to reasonable *sub-concepts*.

To bridge these gaps, we present a supervised post-hoc local-to-global approach for explaining the feature space at the concept level. It essentially unravels the single-step base approach into two steps: (1) Instead of optimizing a single concept vector on a concept dataset, one Guided Concept Projection Vector (GCPVs) is optimized per concept segmentation label in the dataset, locally offering precise label reconstruction (see Fig. 1). These are then (2) generalized to global concept and sub-concept vectors by hierarchical agglomerative (=bottom-up) clustering of GCPVs. This preserves concept distribution over the CNN latent space for further analysis purposes. Furthermore, we introduce a mechanism to extend our method for simultaneous analysis of multiple layers, enhancing the quality of concept generalization. Our key contributions are:

1. A local, i.e., per-sample, method to associate the segmentation label of a semantic concept with a vector in CNN latent space (its GCPV) identifying network units locally encoding concept information;
2. A technique to generalize a concept’s GCPVs to global vector representations (Generalized GCPVs) with superior performance compared to purely global concept analysis approaches, and sub-concept discovery for free;
3. Experimental analysis of influence factors showing the benefit of jointly considering multiple network layers, and robustness to low-resolution concept labels;
4. Demonstration of GCPVs application to several debugging problems, notably concept category confusion and identification of concept-level outliers, offering insights for data and model enhancement.

2. Related Work

Local-to-global Explanations. The field of XAI is vast by now [7, 25, 41, 65, 72], with methods roughly separated into ante- and post-hoc [6, 41, 65]. Ante-hoc methods like concept bottleneck models [8, 9, 36, 44, 73] apply design- and training-time modifications to obtain models with intrinsically transparent representations and/or processing, but often cannot ensure full feature space interpretability [27, 34, 48]. Post-hoc methods, as considered here, instead allow to reveal what an already trained model has learned. For local insights why a single output was obtained, commonly one measures input feature importance, via perturbations [16, 47, 53, 54, 60], gradients [68–71], or as regions with high activation values [66, 79]. Global post-hoc explainability instead aim to derive global properties or interpretable surrogates [28, 57, 77] (“how does the model work”). Only few methods, however, generalize local insights to global ones, allowing to assess the distribution in feature space; a notable example is SpRAY [37], which clusters local feature saliency masks. Unfortunately, besides fidelity issues [2, 21], local feature importance methods do only consider, if at all, CNN information flow, neglecting the knowledge encoded in latent space representations. This lead to (mostly global) concept analysis methods (see next).

Concept-based Explainability. Concept-based methods aim to connect regions in the input space, which can be human-interpreted as specific words or phrases and are often termed semantic concepts [18, 22, 35], with numerical representations in the feature space. Global methods fall into two groups [6, 41, 65]: ante-hoc, and post-hoc methods allow to reveal what an already trained model has learned, as considered here. For qualitative insights, unsupervised post-hoc methods can be used. These employ clustering of activations [20, 22], activation pixel clustering [55, 56], or general matrix factorization [17, 78] to the latent space to obtain reoccurring activation patterns as the learned concepts. These, however, may not be interpretable, are sensitive to quality and diversity of the input data [22, 50]. Supervised post-hoc methods associate latent space representations to user-pre-defined concepts [64]. For example, TCAV [35] and TCAR [13]. They represent image-level concepts as global vectors and radial feature space regions, respectively, but do not allow concept localization. NetDissect [5] and Net2Vec [18] associate concepts with (linear combinations of) convolutional filters and, thus, provide saliency maps for these concepts, though with decreasing accuracy for broad concepts. Also, they face scalability issues for larger models [63]. These baseline ideas remain the basis of all extensions [14, 24, 46, 63, 76]. Besides imprecise local concept localization, existing global concept analysis methods, to our knowledge, do not account for concept variance in latent spaces, potentially overlooking anomalies or incorrectly generalizing complex feature spaces.

Outlier and Anomaly Detection. Anomaly detection aims to identify input objects that are different from the training data distribution. In explainable anomaly detection in CNNs, local feature importance methods such as LIME [10] and SHAP [47], gradient-based ones [62, 66] and LRP [11] are commonly employed. However, these methods have been criticized for their low fidelity and potential inaccuracies in reflecting the anomaly detection process [38]. Additionally, unsupervised post-hoc concept methods [55, 56] are utilized for identifying anomalies. Nevertheless, these methods inherit the limitations of concept discovery techniques discussed earlier.

3. Method Description

To address the issues described before, we propose the post-hoc model-agnostic framework that generates per-sample local explanations from sample activations and concept segmentations (see Fig. 1), and subsequently produces global explanations by generalizing the results of the local explanations. The framework comprises the following steps: (1) for each sample of a training set samples with concept labels, optimize Guided Concept Projection Vector (GCPV) to represent the semantic concepts (Sec. 3.1); (2) apply hierarchical clustering to the GCPVs to reveal the global representation of the concept within the feature space (Sec. 3.2); (3) analyze the resulting hierarchy with respect to quality (Sec. 3.3) to identify significant regions and sub-regions within the feature space, encompassing global representations of concepts, sub-concepts, and concept-level semantic outliers. Additionally, we introduce modifications for simultaneous concept extraction from multiple layers, resulting in improved performance (Sec. 3.4).

3.1. Local GCPVs

Assume we are given an input image x of height and width $h \times w$, a concept label \mathbf{c} as a $h \times w$ -sized binary segmentation mask that localizes the concept occurrences in the image, and a layer L of interest of the CNN f , in which information about the concept label should be found. Now we want to find out whether and how information about \mathbf{c} is distributed over the channels of the layer’s activation maps $f_{\rightarrow L}(x) \in \mathbb{R}^{C \times H \times W}$ (C, H, W the channel, height, width dimensions). Note that the activation map of C can be scaled to represent a non-binary mask for the input using a respective scaling function $p: H \times W \rightarrow h \times w$. Thus, the channel’s information is projected to the input. If these scaled channel masks can be used to reconstruct the ground truth concept mask \mathbf{c} , then (1) the CNN stores information about the concept, (2) the optimal reconstruction quality tells how well it does, and (3) the reconstruction routine—if comparable—serves as a representation of concept information within the CNN.

Formalization. Similar to Net2Vec [18], we aim for reconstruction via linear combination of the channel masks. Thus, our goal formally is: Find a vector $v \in \mathbb{R}^{C \times 1 \times 1}$ of C weights for linearly combining the channel masks such that the resulting *concept projection mask* $P(v; x) \in \mathbb{R}^{h \times w}$ optimally coincides with the concept label mask \mathbf{c} as defined by a loss \mathcal{L} (see Fig. 4). The *Guided Concept Projection Vector (GCPV)* for our concept label is the vector v comprising these optimal linear weights:

$$v = \arg \min_{v \in \mathbb{R}^{C \times 1 \times 1}} \mathcal{L}(v, \mathbf{c}; x) \quad (1)$$

$$\mathcal{L}(v, \mathbf{c}; x) = \mathcal{L}_m(P(v; x), \mathbf{c}) + \mathcal{L}_{\text{reg}}(v) \quad (2)$$

where \mathcal{L}_m and \mathcal{L}_{reg} measure divergence of the masks and regularization respectively, and

$$P(v; x) = p(v \circ f_{\rightarrow L}(x)) = p(\sum_{k \leq C} v_k \cdot f_{\rightarrow L}(x)_k). \quad (3)$$

The GCPV represents the information available in the CNN latent space that allows to localize the concept in the specific input image, and encodes which channels contribute positively, not at all, or negatively to localizing the concept. The important difference to Net2Vec is that optimality shall be achieved for the single given concept label \mathbf{c} , not for a dataset of labels. Compared to [17, 18, 78], we use per-channel weights, thus can use the concept projection masks $P(v; x')$ to visualize the GCPV on any input image x' .

Optimization. To optimize the GCPV v with respect to the loss \mathcal{L} , we initialize the entries of v as 1. This uniform initialization provides equal starting conditions for all channels, emphasizing the enhancement of strong features and the reduction of weaker ones. Before calculating the difference between concept ground truth mask \mathbf{c} and GCPV projection $P(v; x)$, the projection is normalized to values $(0, 1)$ using an element-wise sigmoid $\sigma(z) = 1/(1 + \exp(-z))$. The loss is chosen to be based on mean absolute error (MAE), which equally penalizes low and high differences between any two masks $P, \mathbf{c} \in \mathbb{R}^{h \times w}$:

$$\mathcal{L}_m(P, \mathbf{c}) = \text{MAE}(\sigma(P), \mathbf{c}) = \frac{1}{hw} \sum_{i \leq h, j \leq w} \|\sigma(P_{i,j}) - \mathbf{c}_{i,j}\|_1 \quad (4)$$

Depending on application requirements and objectives, MAE can be substituted with mean square error (MSE) or Dice loss. To promote only channels with strong features and avoid extreme values of v , we also apply L_1 and L_2 regularizations. Thus, the final optimization objective reads as follows:

$$\mathcal{L}_{\text{reg}}(v) = \|v\|_1 + \|v\|_2 \quad (5)$$

$$\mathcal{L}(v, \mathbf{c}; x) = \text{MAE}(\sigma(P(v; x)), \mathbf{c}) + \alpha (\|v\|_1 + \|v\|_2) \quad (6)$$

where $\alpha = \frac{1}{C}$ is a joint-regularization coefficient.

3.2. Generalized Global GCPVs via Clustering

In well-learned feature spaces, samples from the same semantic category activate identical convolutional filters [18]. Therefore, GCPVs corresponding to regions in the input space that represent similar concepts should have similar values. This enables the use of distance-based clustering to explore the concept-level structure of the feature space and obtain generalized global representations from multiple local GCPV of a concept.

Note that neither normalization nor dimensionality reduction can be applied to GCPVs: Normalization can distort comparisons by scaling filter intensity values, and dimensionality reduction for clustering or visualization steps might remove or distort crucial information encoded in the GCPV. Hierarchical clustering, utilizing flexible cluster selection and dendrograms (see Fig. 6), avoids these limitations. We suggest using standard Ward’s linkage agglomerative clustering [74]¹, which minimizes variance within each cluster. This method requires Euclidean distance as distance metric.

Generalized GCPVs. The generation of global or sub-global explanations from a cluster Q of GCPVs is achieved by computing the cluster centroid $\mathbf{v}_Q = \frac{1}{|Q|} \sum_{v \in Q} v$, referred to as Generalized GCPVs (GGCPVs).

Obtaining Clusters. The identification of these GCPV clusters consists of two steps: first the hierarchical clustering to obtain a hierarchy tree of GCPV nodes, and second the cluster selection. The first step follows two scenarios: clustering GCPVs belonging to one or multiple concepts.

Single concept clustering: In this scenario, samples belonging to a single concept are clustered with the aim of uncovering finer details of the concept representation. Clusters are chosen from the hierarchy when their linkage distance exceeds a user-defined threshold. The resulting sub-clusters correspond to sub-concepts within the main concept. For example, a cluster may be subdivided by the aspect of remoteness of the concept in the image as in Fig. 7.

Multiple concepts clustering: Here, diverse semantic categories are examined to assess concept separation in the feature space. Small or impure clusters (e.g., clusters 6, 7, 8 in Fig. 6a) indicate regions with potential semantic outliers or features leading to concept confusion. In particular, the level of concept confusion in the feature space can be determined specifically for similar or easy-to-confuse categories, as illustrated for bus, truck, and car in Fig. 6c.

Once the GCPV hierarchy binary tree is obtained, we can select subtrees of desired granularity as clusters for the explanation. We employ recursive Algorithm 1 for Adaptive Cluster Selection, which traverses the hierarchy from root-to-leaves. For a subtree to be recognized as a cluster, it must pass two quality checks: the cluster purity threshold

Algorithm 1 Adaptive Cluster Selection

```

1: function LINKAGETREETOCLUSTERS(Node)
2:   if Node.IsLeaf then
3:     RememberCluster(Node)
4:   else
5:     if Node.Size < CST then
6:       RememberCluster(Node)
7:     else if Node.Purity > CPT then
8:       RememberCluster(Node)
9:     else
10:      LINKAGETREETOCLUSTERS(Node.left)
11:      LINKAGETREETOCLUSTERS(Node.right)
12:     end if
13:   end if
14: end function

```

(CPT), ensuring a minimum purity (see Eq. (8)), and the cluster size threshold (CST), setting the minimum number of GCPVs per cluster. If a subtree is a leaf, it is also assigned to a cluster. The purity of a cluster Q is measured as the maximum proportion of GCPVs v_c belonging to concept labels c of one concept class $C \in \text{Concepts}$:

$$\text{Purity}(Q) = \frac{1}{|Q|} \max_{C \in \text{Concepts}} |Q \cap V_C| \in [0, 1] \quad (7)$$

with V_C the set of all GCPVs belonging to class C .

Usage of GCPVs on new Samples. A clustering of a set of GCPVs V can be used to assign a concept class to a newly provided concept segmentation \mathbf{c} . For this, first the local GCPV v_c matching \mathbf{c} is obtained as described in Sec. 3.1. We then propose two alternative approaches for assignment of a concept class to v_c :

Affinity to Cluster Centroid: \mathbf{c} is associated with the cluster Q whose GGCPV is nearest to v_c , and we assign the concept class most occurring in Q .

kNN: Using the k nearest neighbors (kNN) approach, the k GCPVs closest to v_c are selected, and \mathbf{c} is assigned the concept class most frequently occurring amongst these.

3.3. Quality Checks for GCPVs

To assess meaningfulness of GGCPVs or GCPVs, a qualitative approach is to manually inspect their projections to given input samples. The resulting masks emphasize regions relevant to the concept encoded in the projection vector (see Fig. 7 and Fig. 5). For a quantitative evaluation, the overall purity of the clustering, as well as its classification performance on new samples may give further insights into clustering quality.

Clustering Quality. To assess the quality of clustering results, i.e., of a partition \mathbf{Q} of the set V of GCPVs, we employ global clustering purity, which measures overall cluster homogeneity on a scale from 0 to 1 as

$$\text{Purity}(\mathbf{Q}) = \frac{1}{|V|} \sum_{Q \in \mathbf{Q}} \max_{C \in \text{Concepts}} |Q \cap V_C| \quad (8)$$

¹<https://docs.scipy.org/doc/scipy/reference/generated/scipy.cluster.hierarchy.ward.html>

and is proportional to the mean of per-cluster purities weighted by cluster size. High purity signifies well-grouped semantically similar samples within the feature space. Clustering purity alone, however, is insufficient, because numerous small clusters with samples of the same concept may be produced. To counter this, we monitor the number of generated clusters $|\mathbf{Q}|$. Ideally, each tested concept should be assigned to a single cluster.

Classification Accuracy. As described in Sec. 3.2, a GCPVs clustering can be used to classify unseen concept segmentations. In case the concept class of the segmentations is known, standard classification metrics like F1-score can be employed to evaluate the performance. Good performance indicates that the found GCPVs clusters each consistently represent a specific human interpretable concept. Bad performance can indicate hard-to-separate concepts, or a bad alignment between the human’s and the CNN’s understanding of a semantic concept and its similarities.

3.4. Multi-layer GCPV

The same semantic information is distributed across numerous layers of CNNs at increasing levels of abstraction [18, 50, 63]. In particular, distinctive differences of concepts may reside in different layers. By analyzing merged information from different depths, we can obtain more precise explanations [17, 55]. We incorporate this insight into our framework.

Assume we have optimized for one input sample and concept label several GCPVs v_i in i different network layers L_i with channel dimensions C_i . To form a Multi-Layer GCPV (MLGCPV), these vectors are concatenated, resulting in the MLGCPV with dimensions $(\sum_i C_i) \times 1 \times 1$ (Fig. 2). Using MLGCPV to represent concept labels in clustering and further analysis allows to respect distribution of concept information over distinct layers.

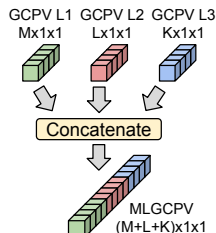


Figure 2. Concatenation of GCPVs into a MLGCPV.

All properties applicable to GCPVs also extend to MLGCPVs, with a notable distinction: the evaluation and visualization of projections. In the case of MLGCPV, multiple projections can be derived (one per used GCPV), and these can be employed individually or averaged for further analysis. Note that the selection of layers depends on the current task and used concepts due to potential differences in their information distribution over layers. Incorporating semantic details from various abstraction levels, MLGCPV offers flexibility in layer selection. This flexibility is crucial in performance-critical applications.

4. Experiments

In our experiments, using the setup outlined in Sec. 4.1, we validate the local and global explanations generated by our method, comparing them both qualitatively and quantitatively with the Net2Vec [18] baseline (Sec. 4.2). Next, in Sec. 4.3, we explore factors affecting the clustering quality. Lastly, in Sec. 4.4, we demonstrate the application of our method in debugging the feature space by detecting concept-level outliers and confusion between semantic categories.

4.1. Experimental Setup

Models and Data. We conduct experiments using object detectors of different and backbones, to evaluate the applicability of our approach: YOLOv5s¹ [33] with residual DarkNet [26, 58] backbone, and SSD² [42], which utilizes a VGG [67] backbone. Models are trained on the semantically rich MS COCO [40]. For testing and concept extraction, we employ the validation subset of MS COCO [40], which provides bounding boxes and segmentations for 80 concepts. To ensure meaningful analysis, we filter out concept samples with segmentation areas less than 2.5% and greater than 80% of the image. This step is taken to avoid instances where no activations or all activations can fit within the optimization criteria, ensuring the reliability of our results. Our experiments specifically target concepts within the ‘vehicle’ and ‘animal’ supercategories. Unless otherwise specified, in individual experiment runs, we sample 100 GCPVs per category for clustering.

GCPVs Optimization and Clustering. GCPV optimization was conducted using AdamW optimizer [45] with default settings at 200 epochs and learning rate of 0.1. For the Adaptive Cluster Selection (see Sec. 3.2 and Algorithm 1) we explore two hyperparameter scenarios for enforcing purity: *relaxed* (CPT = 0.8, CST = 5%) and *strict* for smaller but purer clusters (CPT = 0.9, CST = 2.5%). Here, CST denotes a portion of analyzed samples. To compare GCPVs and MLGCPVs, we conduct experiments both on the single-layer and multi-layer configurations outlined in Tab. 1. We specifically choose layers located near detection heads and intermediate layers, where network branches merge.

Table 1. Layer sets used for experiments in YOLOv5 and SSD.

Model	Set name	Layers		
SSD	S.3	<i>features.21</i>	<i>extra.0.5</i>	<i>extra.1.0</i>
YOLOv5	Y.1	<i>10.conv</i>	—	—
	Y.2	<i>10.conv</i>	<i>20.cv3.conv</i>	—
	Y.3	<i>10.conv</i>	<i>17.cv3.conv</i>	<i>20.cv3.conv</i>

Ground Truth Formats. In practice, high-resolution concept segmentation masks are costly to obtain. As activa-

¹<https://github.com/ultralytics/yolov5>

²<https://pytorch.org/vision/stable/models/ssd>

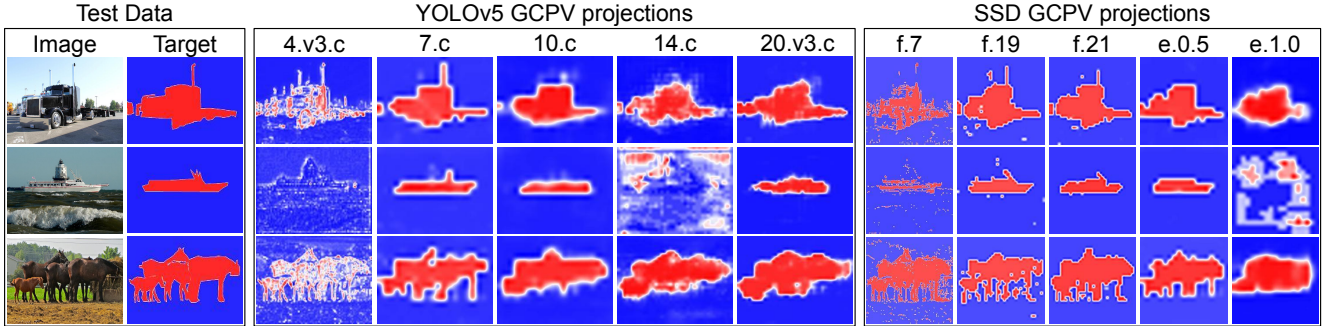


Figure 3. GCPVs projections for target segmentations in different layers of YOLOv5 and SSD (c=conv, v=cv, f=features, e=extra).

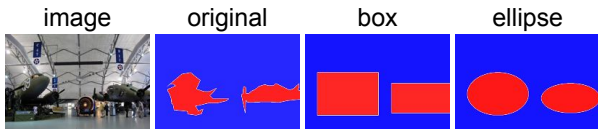


Figure 4. Used ground truth formats for GCPV optimization.

tion maps in deeper layers often have low resolutions, we hypothesize that our method also works with approximate segmentations. We obtain such from cheaper bounding box annotations via box or ellipse pasting as shown in Fig. 4.

4.2. Validation and Baseline Comparison

Projections. Fig. 3 illustrates the projections of GCPVs (see Sec. 3.1) across different layers. Given the high level of abstraction of used concepts, not all layers yield meaningful optimization results. In shallow layers, such as 4.v3.c in YOLOv5 and f.7 in SSD, the model lacks knowledge of the concepts necessary to represent the desired target precisely. In some middle (14.c in YOLOv5) or deep (e.1.0 in SSD) layers, targets might also be beyond the scope, possibly due to changes in receptive fields of layers or the branching structure of the network. Sec. 4.3 investigates whether usage of MLGCPVs mitigate this.

GGCPV versus Net2Vec. Fig. 5 presents the results of comparing the global GGCPVs generated from all concept-related GCPVs with the baseline of global vectors obtained with Net2Vec [18]. Qualitative evaluation of GGCPV and Net2Vec representations in both the 10.conv and extra.1.0 layers of YOLOv5 and SSD networks reveals highly similar concept masks. This observation demonstrates that the global GGCPV, derived by generalizing numerous GCPVs, contain meaningful information and can effectively be employed in explanations.

For a quantitative comparison between global Net2Vec representations and GGCPVs, we assess their projections using baseline segmentation. We calculate the mean Jaccard index (IoU) between ground-truth segmentation masks and binarized projections of all tested category samples. The binarization of projections involves selecting threshold values. Qualitatively, we evaluate the maximum IoU

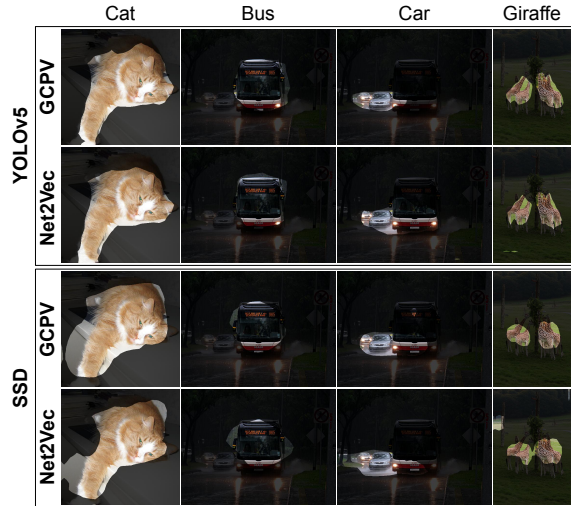


Figure 5. Comparison of concept projections obtained for GGCPVs and Net2Vec in layers 10.conv of YOLOv5 and extra.1.0 of SSD.

Table 2. Quantitative comparison of Net2Vec global representations and GGCPVs for different categories in layer 10.conv of YOLOv5. Best per category **bold**.

Metric	Method	cat	dog	bus	car	plane	zebra	giraffe
max IoU	Net2Vec	0.62	0.37	0.61	0.35	0.46	0.55	0.53
	GCPV	0.64	0.57	0.68	0.46	0.51	0.68	0.52
AUC	Net2Vec	0.22	0.20	0.18	0.11	0.18	0.22	0.15
	GCPV	0.35	0.28	0.41	0.19	0.26	0.40	0.22

achieved for any binarization threshold and the area under the curve (AUC) of the IoU-vs-threshold function. Maximum IoU reflects the overall quality of generated projections, while AUC indicates the consistency of projection quality across different binarization thresholds. Although Net2Vec exhibits scalability issues in larger models [63], the results for YOLOv5 in Tab. 2 demonstrate comparable maximum IoU values, indicating similar global representations. However, the AUC of GGCPVs is higher, indicating a lower sensitivity to the choice of binarization values.

Classification of new Segmentations. For a quantitative sanity check, we assess the capability of our framework to

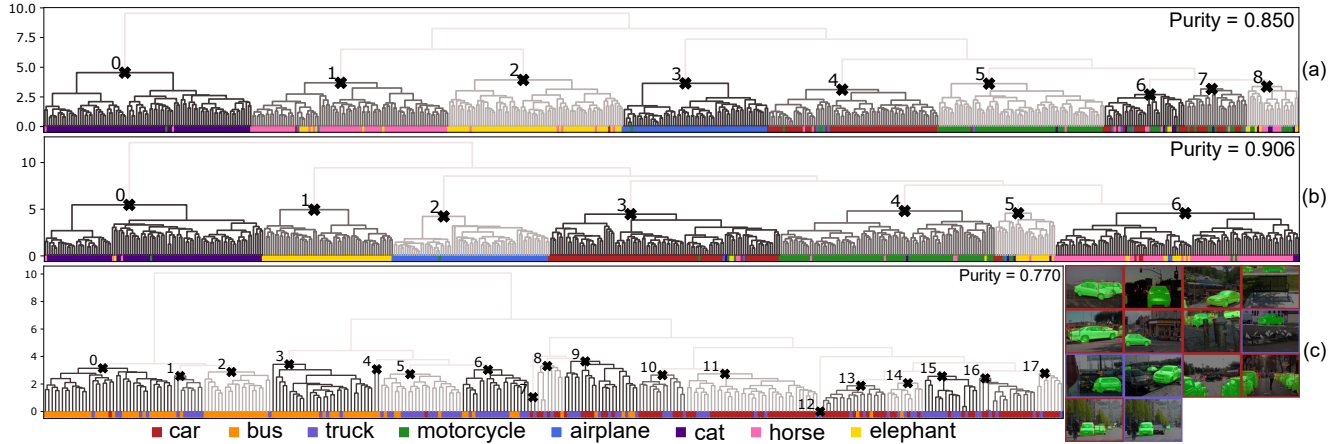


Figure 6. Clustered GCPVs and MLGCPVs sampled using the same seed in the layer sets (see Tab. 1): (a) Y.1 (single-layer); (b) Y.3; (c) Y.3 showing the confusion of concepts *car*, *bus*, *truck* (left) with samples of cluster 10 (right).

Table 3. Mean and standard deviations of MLGCPV clustering quality metrics across 50 runs with varied cluster selection parameters (CPT=Clustering Purity Threshold, CST=Cluster Size Threshold), guides, and layer sets (see Tab. 1) for SSD and YOLOv5 networks.

Clustering	relaxed: CPT = 0.8, CST = 5%						strict: CPT = 0.9, CST = 2.5%					
	Model	YOLOv5					Model	YOLOv5				
Layer set	S.3	Y.1	Y.2	Y.3			S.3	Y.1	Y.2	Y.3		
Guide	original	original	original	original	box	ellipse	original	original	original	original	box	ellipse
Purity	0.84±0.02	0.87±0.01	0.89±0.01	0.90±0.01	0.85±0.02	0.85±0.02	0.86±0.01	0.88±0.01	0.91±0.01	0.91±0.01	0.88±0.01	0.88±0.01
Q	16.3±2.0	10.0±2.1	10.2±1.8	10.2±1.7	10.8±1.9	12.6±2.0	30.2±3.4	20.4±3.2	17.2±2.6	16.9±2.7	21.2±3.1	22.8±2.7

Table 4. Mean and standard deviations of F1-scores of category predictions for new GCPVs and MLGCPVs with kNN and cluster centroid distance in YOLOv5 for 50 runs. Best per row **bold**.

Method	Setup	Layer Sets		
		Y.1	Y.2	Y.3
kNN	k=5	0.857±0.028	0.859±0.030	0.867±0.030
	k=7	0.850±0.029	0.857±0.027	0.862±0.029
	k=9	0.847±0.030	0.853±0.031	0.859±0.032
centroid (GGCPV)	relaxed	0.891±0.026	0.907±0.029	0.907±0.030
	strict	0.893±0.026	0.904±0.026	0.906±0.028

predict the concept class of new segmentations as proposed in Sec. 3.2. GCPVs and MLGCPVs from the categories “car”, “motorcycle”, “airplane”, “cat”, “horse”, and “elephant” were divided at a 4:1 ratio into training and test sets. Averaged mean values and standard deviations of prediction F1-scores for YOLOv5 are provided in Tab. 4. The results indicate that the concept class of test set GCPVs and MLGCPVs can be robustly predicted for various setups, and both using kNN and centroids (GGCPVs) approaches, with slight benefit of the latter. Notably, multi-layer setups (Y.2, Y.3) consistently outperform the single-layer setup (Y.1).

4.3. Influence Factors on Clustering Quality

Next we want to quantitatively assess the impact of using multi-layer GCPVs, approximate ground truth formats, and

purity strictness on the clustering quality (cf. Sec. 3.3).

The number of clusters and purity averaged across 50 runs, are presented in Tab. 3. Clustering dendrograms from one run of the relaxed scenario are depicted for single- and multi-layer scenarios in Fig. 6 (a,b). As anticipated, the relaxed clustering approach consistently resulted in larger and less pure clusters compared to the strict scenario.

GCPV vs. MLGCPV. Utilization of MLGCPVs resulted in superior clustering performance compared to GCPVs (see Y.1, Y.2, and Y.3 sets of YOLOv5). Multi-layer configurations exhibited higher clustering purity and a lower number of clusters |Q|, highlighting the benefits of incorporating multi-layer semantics for clustering quality.

Impact of Label Formats. As expected, the approximate segmentation label formats exhibit lower performance compared to the high-quality original, both with a similar but marginal decrease in purity. The rectangular format outperformed the ellipse one in terms of number of clusters. This implies that the concept information loss of the ellipse approximation is more penalizing than the additional concept noise of rectangles; but both pose a valid alternative to costly high-resolution labels with only marginal performance reduction.

4.4. Applications

In this section we investigate applicability of our framework for diverse introspection and debugging tasks, most notably



Figure 7. Detection of subconcepts within the concept “car” using the GCPV framework in layer 10.conv of YOLOv5. The identified subconcepts are related to the distance from the object.

identifying concept confusion and outliers.

GGCPV for Sub-concept discovery. The GGCPV projections of the single-concept clustering scenario are shown in Fig. 7. Here, using all GCPVs associated with the “car” concept in layer 10.conv of YOLOv5, we identified three distinct sub-concept clusters through thresholding of linkage obtained from hierarchical clustering. These sub-concepts correspond to the distance-based representations of the main concept: “proximate car”, “distant car”, and “car at medium range”. These findings emphasize that this generalization can be parametrized to identify sub-concepts.

Uncovering Concept Confusion. GCPVs encode semantic information specific to defined regions within the input space, allowing us to explain the similarities and differences between samples of similar semantic categories. In Fig. 6c (left), a significant degree of similarity is observed among concept representations of samples belonging to the “car”, “truck”, and “bus” categories of MS COCO. These results were generated using the relaxed clustering setup outlined in Sec. 4.3. Notably, the “truck” concept in MS COCO encompasses a wide range of vehicles, including pickups, vans, and autotrucks. Consequently, clusters distinguishing “car” and “bus” categories contain “truck” infusions. For instance, “car” cluster 10 includes pickup truck samples (Fig. 6c (right)). Moreover, a high number of clusters ($|\mathcal{Q}| = 18$) and relatively low purity (Purity = 0.77) were observed. This confusion within the feature space can propagate across layers and lead to misclassification.

Insights derived from these results can inform dataset improvements, such as category refinement (e.g., separating “truck” into “pickup”, “van”, and “truck” categories).

Detection of Semantic Outliers. Another application of GCPVs is the identification of concept-level semantic outliers in the test data. This can also be seen as detecting concepts where CNNs lack generalization. To achieve this, in relaxed and strict clustering scenarios, we conducted 50 runs and labeled a cluster as “bad” if it failed to meet the thresholding criteria for either scenario (see Sec. 4.3). We



Figure 8. Common hard samples of concepts “motorcycle”, “car”, and “elephant” detected across 50 runs using MLGCPV clustering with strict scenario on layer sets (see Tab. 1) Y.3 of YOLOv5 and S.3 of SSD.

recorded the frequency with which each sample was placed in a “bad” cluster. If a sample was in “bad” cluster in more than 50% of sample draws, we classified it as “hard”.

A closer examination of these “hard” samples allowed us to identify potential outlier samples. Fig. 8 illustrates the intersection of “hard” sample sets for both YOLOv5 and SSD models. In most cases, these samples contain a small portion of tested concepts or small instances (since the experiment did not utilize layers that encode small objects), or they may involve obstructed concepts, which can be naturally challenging.

Feature Space Comparison. Comparing clustering metrics across different models enables us to assess the quality of feature space learning in different layers or even models. The results reveal a minor disparity in purity between Y.3 and S.3 layer sets of YOLOv5 and SSD (see Tab. 3). However, a notable difference is observed in the number of clusters $|\mathcal{Q}|$, indicating that the feature space of SSD is more fragmented on the concept level. This may be one of the reasons for the model’s poorer generalization and overall performance.

5. Conclusion

We have introduced a post-hoc architecture-agnostic local-to-global method for explaining how semantic concepts are encoded and distributed in CNN feature space. This is achieved by first obtaining local concept vectors (GCPVs), which are only in a second step generalized to globally applicable regions in latent space to represent a concept. Furthermore, it proved beneficial to combine GCPVs from multiple layers. Our results suggest that GCPVs and their generalization allow for many relevant applications in CNN debugging, such as discovering sub-concepts, concept category confusion, and semantic outliers, even with low-quality concept labels. Future research may investigate on further applications of our local-to-global approach, including generalization to other tasks and architectures than object detectors, and investigate how to minimize the computational effort of the current per-sample optimization. We hope that our research will serve as a foundation for future investigations in concept-based explainability methods and their use for root cause analysis in CNN debugging.

Acknowledgments

The research leading to these results is funded by the German Federal Ministry for Economic Affairs and Climate Action within the project “KI Wissen – Entwicklung von Methoden für die Einbindung von Wissen in maschinelles Lernen”. The authors would like to thank the consortium for the successful cooperation.

References

- [1] ISO/TC 22/SC 32. ISO/PAS 21448:2019: Road vehicles — Safety of the intended functionality, 2019. [1](#)
- [2] Julius Adebayo, Justin Gilmer, Michael Muelly, Ian Goodfellow, Moritz Hardt, and Been Kim. Sanity checks for saliency maps. *Advances in neural information processing systems*, 31, 2018. [2](#)
- [3] Julius Adebayo, Michael Muelly, Iaria Liccardi, and Been Kim. Debugging tests for model explanations. 33:700–712, 2020. [1](#)
- [4] Alejandro Barredo Arrieta, Natalia Díaz Rodríguez, Javier Del Ser, Adrien Bénéttot, Siham Tabik, Alberto Barredo, Salvador García, Sergio Gil-Lopez, Daniel Molina, Richard Benjamins, Raja Chatila, and Francisco Herrera. Explainable artificial intelligence (XAI): Concepts, taxonomies, opportunities and challenges toward responsible AI. *Information Fusion*, 58:82–115, 2020. [1](#)
- [5] David Bau, Bolei Zhou, Aditya Khosla, Aude Oliva, and Antonio Torralba. Network dissection: Quantifying interpretability of deep visual representations. In *Proc. IEEE conf. computer vision and pattern recognition*, pages 6541–6549, 2017. [1](#), [2](#)
- [6] Francesco Bodria, Fosca Giannotti, Riccardo Guidotti, Francesca Naretto, Dino Pedreschi, and Salvatore Rinzivillo. Benchmarking and survey of explanation methods for black box models. *Data Mining and Knowledge Discovery*, pages 1–60, 2023. [2](#)
- [7] Nadia Burkart and Marco F. Huber. A survey on the explainability of supervised machine learning. *Journal of Artificial Intelligence Research*, 70:245–317, 2021. [2](#)
- [8] Chaofan Chen, Oscar Li, Daniel Tao, Alina Barnett, Cynthia Rudin, and Jonathan Su. This looks like that: Deep learning for interpretable image recognition. In *Advances in Neural Information Processing Systems 32*, pages 8928–8939, 2019. [2](#)
- [9] Zhi Chen, Yijie Bei, and Cynthia Rudin. Concept whitening for interpretable image recognition. *Nature Machine Intelligence*, 2(12):772–782, 2020. [2](#)
- [10] Mei-See Cheong, Mei-Chen Wu, and Szu-Hao Huang. Interpretable stock anomaly detection based on spatio-temporal relation networks with genetic algorithm. *IEEE Access*, 9: 68302–68319, 2021. [3](#)
- [11] Penny Chong, Ngai-Man Cheung, Yuval Elovici, and Alexander Binder. Toward scalable and unified example-based explanation and outlier detection. *IEEE Transactions on Image Processing*, 31:525–540, 2021. [3](#)
- [12] European Commission. Proposal for a regulation of the european parliament and of the council laying down harmonised rules on artificial intelligence (Artificial Intelligence Act) and amending certain union legislative acts, 2021. [1](#)
- [13] Jonathan Crabbé and Mihaela van der Schaar. Concept Activation Regions: A Generalized Framework For Concept-Based Explanations. *Advances in Neural Information Processing Systems*, 35:2590–2607, 2022. [1](#), [2](#)
- [14] Patrick Esser, Robin Rombach, and Bjorn Ommer. A disentangling invertible interpretation network for explaining latent representations. In *Proc. 2020 IEEE Conf. Comput. Vision and Pattern Recognition*, pages 9220–9229. IEEE, 2020. [2](#)
- [15] European Commission High-Level Expert Group on Artificial Intelligence (AI HLEG). Assessment List for Trustworthy Artificial Intelligence (ALTAI) for self-assessment. Technical Report 68342, 2020. [1](#)
- [16] Thomas Fel, Rémi Cadène, Mathieu Chalvidal, Matthieu Cord, David Vigouroux, and Thomas Serre. Look at the variance! efficient black-box explanations with sobol-based sensitivity analysis. *Advances in Neural Information Processing Systems*, 34:26005–26014, 2021. [2](#)
- [17] Thomas Fel, Agustin Picard, Louis Bethune, Thibaut Boissin, David Vigouroux, Julien Colin, Rémi Cadène, and Thomas Serre. Craft: Concept recursive activation factorization for explainability. In *Proceedings of the IEEE/CVF Conference on Computer Vision and Pattern Recognition*, pages 2711–2721, 2023. [1](#), [2](#), [3](#), [5](#)
- [18] Ruth Fong and Andrea Vedaldi. Net2vec: Quantifying and explaining how concepts are encoded by filters in deep neural networks. In *Proceedings of the IEEE conference on computer vision and pattern recognition*, pages 8730–8738, 2018. [1](#), [2](#), [3](#), [4](#), [5](#), [6](#)
- [19] Fabian B. Fuchs, Oliver Groth, Adam R. Kosiorek, Alex Bewley, Markus Wulfmeier, Andrea Vedaldi, and Ingmar Posner. Neural Stethoscopes: Unifying analytic, auxiliary and adversarial network probing. *CoRR*, abs/1806.05502, 2018. [2](#)
- [20] Yunhao Ge, Yao Xiao, Zhi Xu, Meng Zheng, Srikrishna Karanam, Terrence Chen, Laurent Itti, and Ziyang Wu. A peek into the reasoning of neural networks: Interpreting with structural visual concepts. In *Proceedings of the IEEE/CVF Conference on Computer Vision and Pattern Recognition*, pages 2195–2204, 2021. [2](#)
- [21] Amirata Ghorbani, Abubakar Abid, and James Zou. Interpretation of neural networks is fragile. In *Proceedings of the AAAI conference on artificial intelligence*, pages 3681–3688, 2019. [2](#)
- [22] Amirata Ghorbani, James Wexler, James Y Zou, and Been Kim. Towards automatic concept-based explanations. *Advances in Neural Information Processing Systems*, 32, 2019. [1](#), [2](#)
- [23] Bryce Goodman and Seth Flaxman. European union regulations on algorithmic decision-making and a “right to explanation”. *AI Magazine*, 38(3):50–57, 2017. [1](#)
- [24] Mara Graziani, Vincent Andrearczyk, and Henning Müller. Regression concept vectors for bidirectional explanations in

- histopathology. In *Understanding and Interpreting Machine Learning in Medical Image Computing Applications*, pages 124–132. Springer International Publishing, 2018. [2](#)
- [25] Riccardo Guidotti, Anna Monreale, Dino Pedreschi, and Fosca Giannotti. Principles of Explainable Artificial Intelligence. In *Explainable AI Within the Digital Transformation and Cyber Physical Systems: XAI Methods and Applications*, pages 9–31. Springer International Publishing, 2021. [2](#)
- [26] Kaiming He, Xiangyu Zhang, Shaoqing Ren, and Jian Sun. Deep residual learning for image recognition. In *Proc. IEEE conf. computer vision and pattern recognition*, pages 770–778, 2016. [5](#)
- [27] Adrian Hoffmann, Claudio Fanconi, Rahul Rade, and Jonas Kohler. This Looks Like That... Does it? Shortcomings of Latent Space Prototype Interpretability in Deep Networks. *arXiv:2105.02968 [cs]*, 2021. [2](#)
- [28] Fred Hohman, Haekyu Park, Caleb Robinson, and Duen Horng Polo Chau. Summit: Scaling Deep Learning Interpretability by Visualizing Activation and Attribution Summarizations. *IEEE Transactions on Visualization and Computer Graphics*, 26(1):1096–1106, 2020. [2](#)
- [29] Sebastian Houben, Stephanie Abrecht, Maram Akila, Andreas Bär, Felix Brockherde, Patrick Feifel, Tim Fingscheidt, Sujan Sai Gannamaneni, Seyed Eghbal Ghobadi, Ahmed Hammam, Anselm Haselhoff, Felix Hauser, Christian Heinzemann, Marco Hoffmann, Nikhil Kapoor, Falk Kappel, Marvin Klingner, Jan Kronenberger, Fabian Küppers, Jonas Löhdefink, Michael Mlynarski, Michael Mock, Firas Mualla, Svetlana Pavlitskaya, Maximilian Poretschkin, Alexander Pohl, Varun Ravi-Kumar, Julia Rosenzweig, Matthias Rottmann, Stefan Rüping, Timo Sämann, Jan David Schneider, Elena Schulz, Gesina Schwalbe, Joachim Sickling, Toshika Srivastava, Serin Varghese, Michael Weber, Sebastian Wirkert, Tim Wirtz, and Matthias Woehrle. Inspect, understand, overcome: A survey of practical methods for AI safety. In *Deep Neural Networks and Data for Automated Driving: Robustness, Uncertainty Quantification, and Insights Towards Safety*, pages 3–78. Springer International Publishing, 2022. [1](#)
- [30] ISO/IEC JTC 1/SC 42 Artificial Intelligence. *ISO/IEC TR 24028:2020 Information Technology — Artificial Intelligence — Overview of Trustworthiness in Artificial Intelligence*. ISO, 1 edition, 2020. [1](#)
- [31] ISO/IEC JTC 1/SC 42 Artificial Intelligence. *ISO/IEC TR 5469:202x(E) - Artificial Intelligence — Functional Safety and AI Systems*. ISO, 202x(e) (working draft) edition, 2021.
- [32] ISO/TC 22/SC 32. *ISO/AWI PAS 8800(En): Road Vehicles — Safety and Artificial Intelligence*. ISO, wd01 edition, 2022. [1](#)
- [33] Glenn Jocher. YOLOv5 in PyTorch, ONNX, CoreML, TFLite. <https://github.com/ultralytics/yolov5>, 2020. [5](#)
- [34] Dmitry Kazhdan, Boty Dimanov, Helena Andres Terre, Mateja Jamnik, Pietro Liò, and Adrian Weller. Is disentanglement all you need? Comparing concept-based & disentanglement approaches. *CoRR*, abs/2104.06917, 2021. [2](#)
- [35] Been Kim, Martin Wattenberg, Justin Gilmer, Carrie Cai, James Wexler, Fernanda Viegas, et al. Interpretability beyond feature attribution: Quantitative testing with concept activation vectors (tcav). In *International conference on machine learning*, pages 2668–2677. PMLR, 2018. [1](#), [2](#)
- [36] Pang Wei Koh, Thao Nguyen, Yew Siang Tang, Stephen Mussmann, Emma Pierson, Been Kim, and Percy Liang. Concept bottleneck models. In *Int. conf. Machine Learning*, pages 5338–5348. PMLR, 2020. [2](#)
- [37] Sebastian Lapuschkin, Stephan Wäldchen, Alexander Binder, Grégoire Montavon, Wojciech Samek, and Klaus-Robert Müller. Unmasking Clever Hans predictors and assessing what machines really learn. *Nature Communications*, 10(1):1096, 2019. [2](#)
- [38] Zhong Li, Yuxuan Zhu, and Matthijs Van Leeuwen. A survey on explainable anomaly detection. *ACM Transactions on Knowledge Discovery from Data*, 18(1):1–54, 2023. [3](#)
- [39] Yu Liang, Siguang Li, Chungang Yan, Maozhen Li, and Changjun Jiang. Explaining the black-box model: A survey of local interpretation methods for deep neural networks. *Neurocomputing*, 419:168–182, 2021. [1](#)
- [40] Tsung-Yi Lin, Michael Maire, Serge Belongie, James Hays, Pietro Perona, Deva Ramanan, Piotr Dollár, and C Lawrence Zitnick. Microsoft coco: Common objects in context. In *European conf. computer vision*, pages 740–755. Springer, 2014. [5](#)
- [41] Pantelis Linardatos, Vasilis Papastefanopoulos, and Sotiris Kotsiantis. Explainable ai: A review of machine learning interpretability methods. *Entropy*, 23(1):18, 2021. [2](#)
- [42] Wei Liu, Dragomir Anguelov, Dumitru Erhan, Christian Szegedy, Scott Reed, Cheng-Yang Fu, and Alexander C Berg. Ssd: Single shot multibox detector. In *Computer Vision—ECCV 2016: 14th European Conference, Amsterdam, The Netherlands, October 11–14, 2016, Proceedings, Part I 14*, pages 21–37. Springer, 2016. [5](#)
- [43] Luca Longo, Mario Brcic, Federico Cabitza, Jaesik Choi, Roberto Confalonieri, Javier Del Ser, Riccardo Guidotti, Yoichi Hayashi, Francisco Herrera, Andreas Holzinger, Richard Jiang, Hassan Khosravi, Freddy Lecue, Gianclaudio Malgieri, Andrés Páez, Wojciech Samek, Johannes Schneider, Timo Speith, and Simone Stumpf. Explainable artificial intelligence (xai) 2.0: A manifesto of open challenges and interdisciplinary research directions, 2023. [1](#)
- [44] Max Losch, Mario Fritz, and Bernt Schiele. Interpretability beyond classification output: Semantic bottleneck networks. In *Proc. 3rd ACM Computer Science in Cars Symp. Extended Abstracts*, 2019. [2](#)
- [45] Ilya Loshchilov and Frank Hutter. Decoupled Weight Decay Regularization. In *International Conference on Learning Representations*, 2018. [5](#), [1](#)
- [46] Adriano Lucieri, Muhammad Naseer Bajwa, Andreas Dengel, and Sheraz Ahmed. Explaining AI-based decision support systems using concept localization maps. In *Neural Information Processing*, pages 185–193. Springer International Publishing, 2020. [2](#)
- [47] Scott M Lundberg and Su-In Lee. A unified approach to interpreting model predictions. *Advances in neural information processing systems*, 30, 2017. [1](#), [2](#), [3](#)

- [48] Emanuele Marconato, Andrea Passerini, and Stefano Teso. GlanceNets: Interpretable, Leak-proof Concept-based Models. In *Advances in Neural Information Processing Systems*, pages 21212–21227, 2022. [2](#)
- [49] Georgii Mikriukov, Gesina Schwalbe, Christian Hellert, and Korinna Bade. Evaluating the stability of semantic concept representations in cnns for robust explainability. *arXiv preprint arXiv:2304.14864*, 2023. [2](#), [1](#)
- [50] Georgii Mikriukov, Gesina Schwalbe, Christian Hellert, and Korinna Bade. Quantified semantic comparison of convolutional neural networks. *arXiv preprint arXiv:2305.07663*, 2023. [2](#), [5](#)
- [51] Daniel Müllner. fastcluster: Fast hierarchical, agglomerative clustering routines for r and python. *Journal of Statistical Software*, 53:1–18, 2013. [1](#)
- [52] W. James Murdoch, Chandan Singh, Karl Kumbier, Reza Abbasi-Asl, and Bin Yu. Definitions, methods, and applications in interpretable machine learning. *Proceedings of the National Academy of Sciences*, 116(44):22071–22080, 2019. [1](#)
- [53] Paul Novello, Thomas Fel, and David Vigouroux. Making sense of dependence: Efficient black-box explanations using dependence measure. *Advances in Neural Information Processing Systems*, 35:4344–4357, 2022. [2](#)
- [54] Vitali Petsiuk, Abir Das, and Kate Saenko. Rise: Randomized input sampling for explanation of black-box models. *arXiv preprint arXiv:1806.07421*, 2018. [2](#)
- [55] Andres Felipe Posada-Moreno, Nikita Surya, and Sebastian Trimpe. Eclad: Extracting concepts with local aggregated descriptors. *arXiv preprint arXiv:2206.04531*, 2022. [1](#), [2](#), [3](#), [5](#)
- [56] Andrés Felipe Posada-Moreno, Kai Müller, Florian Brilowski, Friedrich Solowjow, Thomas Gries, and Sebastian Trimpe. Scalable concept extraction in industry 4.0. *arXiv preprint arXiv:2306.03551*, 2023. [2](#), [3](#)
- [57] Johannes Rabold, Gesina Schwalbe, and Ute Schmid. Expressive explanations of DNNs by combining concept analysis with ILP. In *KI 2020: Advances in Artificial Intelligence*, pages 148–162. Springer International Publishing, 2020. [2](#)
- [58] Joseph Redmon and Ali Farhadi. Yolov3: An incremental improvement. *arXiv preprint arXiv:1804.02767*, 2018. [5](#)
- [59] Marco Tulio Ribeiro, Sameer Singh, and Carlos Guestrin. "why should i trust you?" explaining the predictions of any classifier. In *Proceedings of the 22nd ACM SIGKDD international conference on knowledge discovery and data mining*, pages 1135–1144, 2016. [1](#)
- [60] Marco Túlio Ribeiro, Sameer Singh, and Carlos Guestrin. "Why should I trust you?": Explaining the predictions of any classifier. In *Proc. 22nd ACM SIGKDD Int. Conf. Knowledge Discovery and Data Mining*, pages 1135–1144. ACM, 2016. [2](#)
- [61] Cynthia Rudin. Stop explaining black box machine learning models for high stakes decisions and use interpretable models instead. *Nature Machine Intelligence*, 1(5):206–215, 2019. [1](#)
- [62] Mao Saeki, Jun Ogata, Masahiro Murakawa, and Tetsuji Ogawa. Visual explanation of neural network based rotation machinery anomaly detection system. In *2019 IEEE International Conference on Prognostics and Health Management (ICPHM)*, pages 1–4. IEEE, 2019. [3](#)
- [63] Gesina Schwalbe. Verification of size invariance in DNN activations using concept embeddings. In *Artificial Intelligence Applications and Innovations*, pages 374–386. Springer International Publishing, 2021. [1](#), [2](#), [5](#), [6](#)
- [64] Gesina Schwalbe. Concept Embedding Analysis: A Review. *arXiv:2203.13909 [cs, stat]*, 2022. [1](#), [2](#)
- [65] Gesina Schwalbe and Bettina Finzel. A comprehensive taxonomy for explainable artificial intelligence: a systematic survey of surveys on methods and concepts. *Data Mining and Knowledge Discovery*, pages 1–59, 2023. [2](#)
- [66] Ramprasaath R Selvaraju, Michael Cogswell, Abhishek Das, Ramakrishna Vedantam, Devi Parikh, and Dhruv Batra. Grad-cam: Visual explanations from deep networks via gradient-based localization. In *Proceedings of the IEEE international conference on computer vision*, pages 618–626, 2017. [2](#), [3](#)
- [67] Karen Simonyan and Andrew Zisserman. Very deep convolutional networks for large-scale image recognition. *arXiv preprint arXiv:1409.1556*, 2014. [5](#)
- [68] Karen Simonyan, Andrea Vedaldi, and Andrew Zisserman. Deep inside convolutional networks: Visualising image classification models and saliency maps. *arXiv preprint arXiv:1312.6034*, 2013. [2](#)
- [69] Daniel Smilkov, Nikhil Thorat, Been Kim, Fernanda Viégas, and Martin Wattenberg. Smoothgrad: removing noise by adding noise. *arXiv preprint arXiv:1706.03825*, 2017.
- [70] Jost Tobias Springenberg, Alexey Dosovitskiy, Thomas Brox, and Martin Riedmiller. Striving for simplicity: The all convolutional net. *arXiv preprint arXiv:1412.6806*, 2014.
- [71] Mukund Sundararajan, Ankur Taly, and Qiqi Yan. Axiomatic attribution for deep networks. In *International conference on machine learning*, pages 3319–3328. PMLR, 2017. [2](#)
- [72] Giulia Vilone and Luca Longo. Explainable artificial intelligence: A systematic review. *CoRR*, abs/2006.00093, 2020. [2](#)
- [73] Jiaqi Wang, Huafeng Liu, Xinyue Wang, and Liping Jing. Interpretable image recognition by constructing transparent embedding space. In *Proceedings of the IEEE/CVF International Conference on Computer Vision*, pages 895–904, 2021. [2](#)
- [74] Joe H Ward Jr. Hierarchical grouping to optimize an objective function. *Journal of the American statistical association*, 58(301):236–244, 1963. [4](#)
- [75] Chih-Kuan Yeh, Been Kim, Sercan Arik, Chun-Liang Li, Tomas Pfister, and Pradeep Ravikumar. On completeness-aware concept-based explanations in deep neural networks. In *Advances in Neural Information Processing Systems 33*, pages 20554–20565, 2020. [1](#)
- [76] Mert Yuksekgonul, Maggie Wang, and James Zou. Post-hoc Concept Bottleneck Models. In *ICLR 2022 Workshop on PAIR2Struct: Privacy, Accountability, Interpretability, Robustness, Reasoning on Structured Data*, 2022. [2](#)
- [77] Quanshi Zhang, Ruiming Cao, Feng Shi, Ying Nian Wu, and Song-Chun Zhu. Interpreting CNN knowledge via an ex-

- planatory graph. In *Proc. 32nd AAAI Conf. Artificial Intelligence*, pages 4454–4463. AAAI Press, 2018. [2](#)
- [78] Ruihan Zhang, Prashan Madumal, Tim Miller, Krista A Ehinger, and Benjamin IP Rubinstein. Invertible concept-based explanations for cnn models with non-negative concept activation vectors. In *Proceedings of the AAAI Conference on Artificial Intelligence*, pages 11682–11690, 2021. [1](#), [2](#), [3](#)
- [79] Bolei Zhou, Aditya Khosla, Àgata Lapedriza, Aude Oliva, and Antonio Torralba. Learning deep features for discriminative localization. In *Proc. 2016 IEEE Conf. Comput. Vision and Pattern Recognition*, pages 2921–2929. IEEE Computer Society, 2016. [2](#)
- [80] Jianlong Zhou, Amir H. Gandomi, Fang Chen, and Andreas Holzinger. Evaluating the quality of machine learning explanations: A survey on methods and metrics. *Electronics*, 10(5):593, 2021. [1](#)

GCPV: Guided Concept Projection Vectors for the Explainable Inspection of CNN Feature Spaces

Supplementary Material

A. Limitations

The GCPV method generates human-interpretable visual explanations, but, as is common in post-hoc XAI, quantitatively assessing the accuracy of these explanations remains challenging [43]. Furthermore, the absence of standardized methodologies and the diverse array of approaches employed in XAI make it difficult to conduct an objective and comprehensive comparison with other methods.

The proposed framework inherits the challenges associated with other post-hoc supervised concept-based approaches [5, 13, 18, 35]. GCPVs require high-quality data and labels, a challenge we partially address by introducing alternative segmentation labels (see Sec. 4.3). However, this solution compromises explanation quality.

Additionally, the quality of extracted concepts depends on various initial conditions, such as model architecture, data, and layer selection [49]: we observed instances where GCPV optimization failed in certain layers (see Fig. 3), making comparing such samples unfeasible. To overcome this, we proposed using MLGCPVs.

Unlike unsupervised approaches, supervised methods show *user-defined* information [18, 35], whereas unsupervised methods reveal information *seen by the model* [17, 22]. It is challenging to quantify the disparity between human and machine perspectives. Therefore, a combined use of unsupervised and supervised methods is recommended.

Currently, the GCPV method demands more computational resources than alternative post-hoc baselines [5, 13, 18]. This increased demand arises due to two main factors. Firstly, we employ per-sample concept optimization instead of global concept-wise optimization. Secondly, optimal hierarchical clustering methods have a time complexity of $O(N^2)$ and memory complexity $\Omega(n^2)$ [51]. We acknowledge these computational bottlenecks as potential areas for future research.

Finally, we recognize the potential for enhancing optimization algorithms and objectives in our methodology. While we employed fundamental methods to ensure functionality and versatility, the use of AdamW [45] and MAE objective (see Sec. 3.1) might yield sub-optimal outcomes. Therefore, a more extensive exploration of optimization techniques and their performance is required.

B. Additional Results

GGCPV versus Net2Vec. Fig. 9 demonstrates additional results of the global GGCPVs and baseline Net2Vec [18]

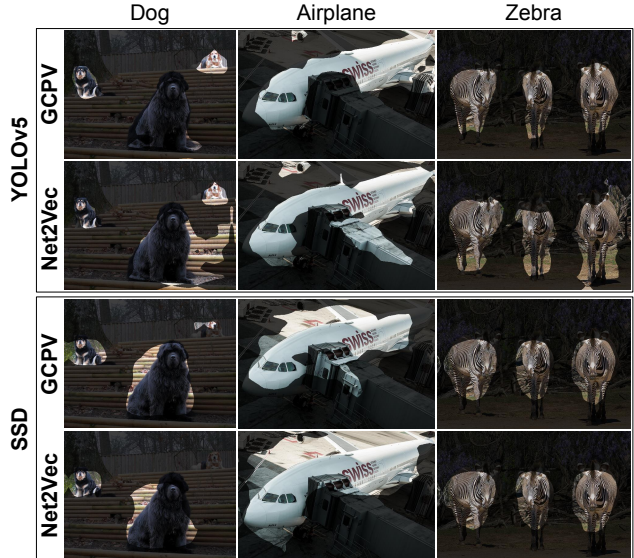


Figure 9. Comparison of concept projections obtained for GGCPVs and Net2Vec in layers *10.conv* of YOLOv5 and *extra.1.0* of SSD.

Table 5. Quantitative comparison of Net2Vec global representations and GGCPVs for different categories in layer *extra.1.0* of SSD. Best per category **bold**.

Metric	Method	cat	dog	bus	car	plane	zebra	giraffe
max IoU	Net2Vec	0.39	0.38	0.62	0.45	0.30	0.60	0.23
	GCPV	0.55	0.53	0.62	0.43	0.43	0.59	0.41
AUC	Net2Vec	0.21	0.20	0.20	0.13	0.09	0.27	0.11
	GCPV	0.31	0.29	0.38	0.21	0.17	0.33	0.15

qualitative comparison in the *10.conv* and *extra.1.0* layers of YOLOv5 and SSD networks. Similar to Sec. 4.2, GGCPVs were generated from all concept-related GCPVs of semantic categories "dog," "airplane," and "zebra." Both GGCPV and Net2Vec representations produce similar masks for additional concepts. This finding reaffirms that the information contained in GGCPVs is meaningful.

In addition to the quantitative comparison of GGCPVs and Net2Vec global vectors in Tab. 2 for YOLOv5, we present similar estimates for SSD in Tab. 5. Despite the mentioned scalability issues of the Net2Vec baseline [63], the behavior of the measured IoU and AUC (discussed in Sec. 4.2) in SSD mirrors what was observed in YOLOv5: the maximum IoU values are comparable, while the AUC of GGCPVs is higher.

Fig. 10 illustrates the IoU-vs-threshold curves used to

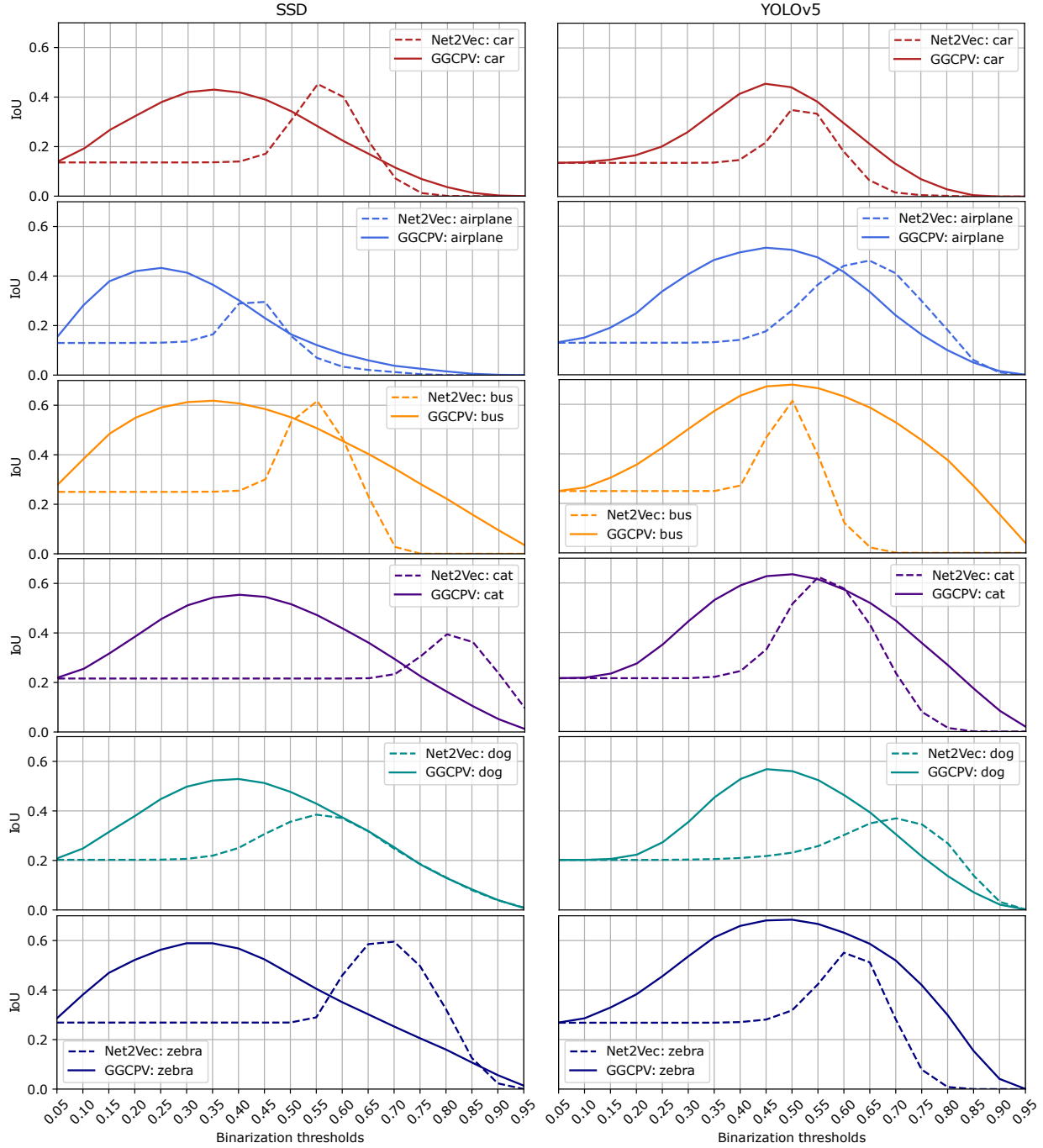


Figure 10. IoU-vs.-threshold diagrams of concepts “car”, “airplane”, “bus”, “cat”, “dog”, and “zebra” for GGCPVs and Net2Vec in layers $10.conv$ of YOLOv5 and $extra.1.0$ of SSD.

evaluate maximum IoU and AUC values. In addition to the results described in Tabs. 2 and 5, it is noteworthy that, in the majority of cases, the maximum IoU value of GCPV is achieved with lower binarization thresholds. This indicates that GCPV representations are less noisy. Specifically, saliency maps obtained for lower values of binarization thresholds from Net2Vec global representations high-

light more concept-unrelated information than these for GCPV, thereby reducing the total per-category IoU between ground truth segmentations and binarized saliency maps. Furthermore, the IoU-vs.-threshold curves for Net2Vec exhibit steeper slopes and more pronounced peak values, making them more sensitive to the selection of optimal binarization threshold.

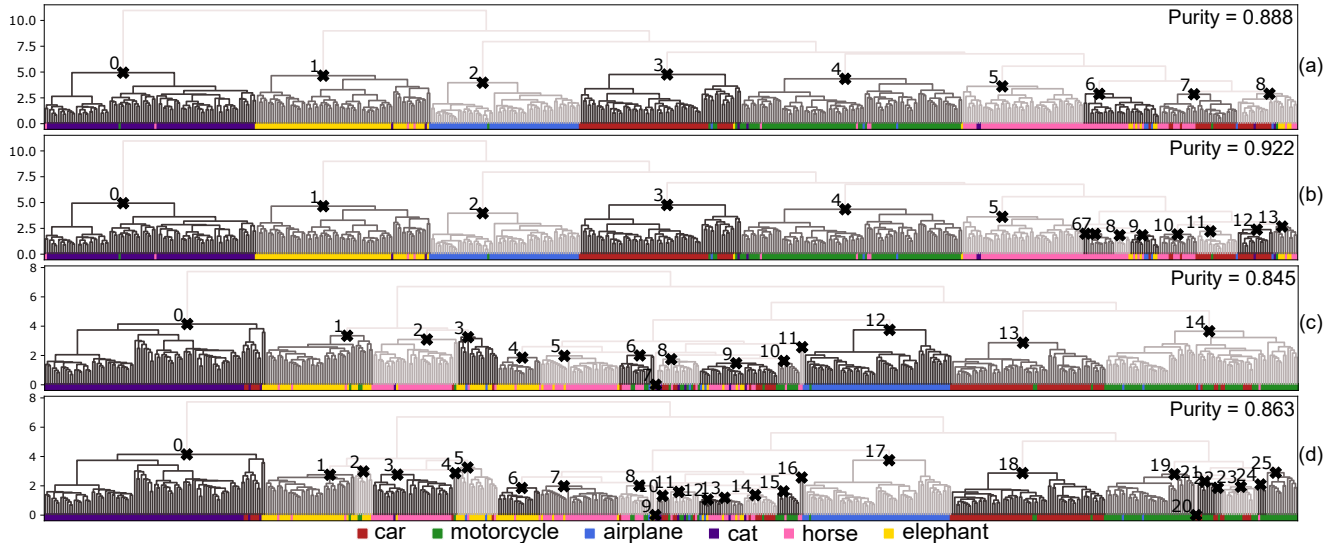


Figure 11. Clustered MLGCPVs sampled using the same seed in different layer sets and scenarios (see Tab. 1 and Sec. 4.3): (a) Y.2 relaxed; (b) Y.2 strict; (c) S.3 relaxed; (d) S.3 strict.

Table 6. Mean and standard deviations of F1-scores of category predictions for new MLGCPVs with kNN and cluster centroid distance in SSD for 50 runs. Best per row **bold**.

Method	Setup	Layer Set
		S.3
kNN	k=5	0.729±0.031
	k=7	0.736±0.028
	k=9	0.741±0.031
centroid (GGCPV)	relaxed	0.817±0.031
	strict	0.836±0.032

Classification of new Segmentations. Tab. 6 extends the results of Tab. 4. It displays the MLGCPV semantic category prediction for the categories “car”, “motorcycle”, “airplane”, “cat”, “horse”, and “elephant” for S.3 of SSD under the conditions described in Sec. 4.2. Similar to the results for YOLOv5 (Tab. 4), the results for SSD indicate that the prediction of semantic categories is possible. However, due to the more fragmented structure of the SSD feature space compared to YOLOv5, which is evident from Fig. 11 (a, c) and Tab. 3, the overall performance of such prediction is lower for SSD.

Impact of Clustering Scenarios. Fig. 11 presents additional clustering dendrograms for the same samples utilized in Fig. 6 (a, b). These illustrations showcase the impact of clustering scenario selection, as discussed in Sec. 4.3, on cluster assignments for the Y.2 (a, b) and S.3 (c, d) layer setups (see Tab. 1). Notably, the relaxed scenario (a, c) yields fewer clusters with lower purity than the strict one (b, d). For instance, (c) exhibits 15 clusters with an overall purity of 0.845, whereas (d) comprises 26 clusters with a purity of

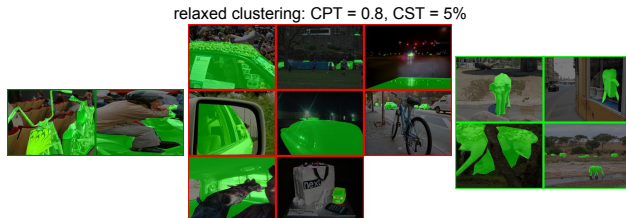


Figure 12. Common hard samples of concepts “motorcycle”, “car”, and “elephant” detected across 50 runs using MLGCPV clustering with relaxed SSD scenario on layer sets (see Tab. 1) Y.3 of YOLOv5 and S.3 of SSD.

0.863. Under strict conditions, specific regions of the feature space are more finely divided, such as the region with clusters 6-8 in (a) and 6-13 in (b) or cluster 14 in (c) and clusters 19-25 in (d).

Detection of Semantic Outliers. Fig. 12 extends the experiment discussed in Sec. 4.4. It illustrates the intersection of “hard” sample sets for YOLOv5 Y.3 and SSD S.3 under a relaxed clustering scenario, as detailed in Sec. 4.3. The primary distinction from the strict scenario results (see Fig. 8) is the reduced number of samples classified as “hard”. This reduction is due to the larger tolerance for impurities in clusters in the relaxed scenario compared to the strict one. Consequently, for the identification of semantic outliers, we recommend utilizing stricter clustering threshold CPT and CST (see Sec. 3.2) with Algorithm 1.